Original Article

Semiautomated Three-Dimensional Landmark Placement on Knee Models Is a Reliable Method to Describe Bone Shape and Alignment

Nancy Park, B.S., Johannes Sieberer, M.Sc., Armita Manafzadeh, Ph.D., Rieke-Marie Hackbarth, Shelby Desroches, B.S., Rithvik Ghankot, B.S., John Lynch, Ph.D., Neil A. Segal, M.D., Joshua Stefanik, Ph.D., David Felson, M.D., and John P. Fulkerson, M.D.

Purpose: To assess the inter- and intrarater reliability of 21 anatomical landmarks initially placed with an artificial intelligence algorithm and then manually verified with human input. **Methods:** Thirty computed tomography scans of the knees of participants from the Multicenter Osteoarthritis Study (MOST) ages 45 to 55 years were included. Approximately one-half experienced progression of patellofemoral osteoarthritis, defined as an increased cartilage score in the patellofemoral compartment on magnetic resonance imaging over 2 years. The algorithm automatically placed 19 anatomic landmarks on the femur, tibia, and patella. An additional 2 landmarks were added manually. Two landmark reviewers separately reviewed all 30 scans and verified all landmarks. After 2 weeks, one reviewer repeated the process for the same dataset. The mean Euclidean distance of manual landmark displacement, mean absolute disagreement between and within raters, and intraclass correlation coefficients for inter- and intrarater reliability were calculated. **Results:** All landmarks had excellent inter-rater reliability. The tibial and femoral shaft centers had intraclass correlation coefficients (ICCs) of 1, indicating their positions did not differ. Seventeen landmarks had ICCs between 0.90 and 0.99 and the tibial tuberosity had an ICC of 0.87. Intrarater reliability scores were 1 for 16 landmarks and between 0.90 and 0.99 for the remaining 5. **Conclusions:** There was excellent agreement on the locations of all 21 landmarks evaluated in this study. **Clinical Relevance:** The potential role of artificial intelligence in medical imaging and orthopaedic research is a growing area of interest. The excellent reliability demonstrated across multiple landmarks in our study reveals the potential for semiautomated 3-dimensional methods to enhance precision of anatomical measurements of the knee over 2-dimensional methods.

Anatomic metrics, or quantified descriptions of anatomic relationships, are pivotal in understanding factors that drive the development of different musculoskeletal conditions. Many anatomic metrics were developed before comprehensive analysis using 3-dimensional (3D) reproductions were available. Typically, 2-dimensional (2D) radiographic or slice-by-slice analysis of computed tomography (CT) and magnetic resonance imaging (MRI) scans are used to localize landmarks. Simplifying the knee from 3 dimensions to 2 can distort the nature of its bony architecture. For example, tibial tubercle-trochlear groove (TT-TG) distance describes the distance between the TT and the TG.[1] In this case, the TT and TG are 2 anatomic landmarks that mark easily identifiable features of the knee. TT-TG can be subject to distortions because of leg positioning or slice selection, muddling its interpretation and utility for surgical decision making.[2-4]

Anatomic metrics generally describe the geometrical relationship between anatomic landmarks with some metrics sharing common landmarks. As a result, identifying all required landmarks and algorithmically

From Yale University, New Haven, Connecticut, U.S.A. (N.P., J.Si., A.M., R-M.H., S.D., R.G., D.F., J.P.F.); University Medical Center Hamburg-Eppendorf, Hamburg, Germany (R-M.H.); Department of Epidemiology and Biostatistics, University of California, San Francisco, San Francisco, California, U.S.A. (J.L.); Department of Physical Medicine and Rehabilitation, University of Kansas Medical Center, Kansas City, Kansas, U.S.A. (N.A.S.); Department of Physical Therapy, Human Movement, and Rehabilitation Sciences, Northeastern University, Boston, Massachusetts, U.S.A. (J.St.); and Section of Rheumatology, Department of Medicine, Boston University School of Medicine, Boston, Massachusetts, U.S.A. (D.F.).

N.P. and J.S. contributed equally as cofirst authors.

Received July 25, 2024; accepted October 14, 2024.

Address correspondence to Nancy Park, B.S., Department of Orthopaedics and Rehabilitation, Yale School of Medicine, 47 College St., New Haven, CT 06510, U.S.A. E-mail: Nancy.park@yale.edu

2666-061X/24958

https://doi.org/10.1016/j.asmr.2024.101036

calculating all corresponding metrics would be a more efficient method. For example, the posterior condylar line of the femur is used as a reference axis in measuring patellar tilt, TT-TG, and lateral trochlear inclination. Determining the location of the 2 posterior condyles would readily enable calculation of the reference axis for all 3 metrics. Artificial intelligence (AI) models for translating medical images into 3D models that can identify anatomic landmarks have already been developed, allowing for even more automation.

Previous statistical shape analysis studies have used bone surface landmarks to calculate the bone shape of the patella and femur in 3D space.[5,6] For example, Williams et al.[7] describes using bone shape on 3D MRI to predict preosteoarthritis after anterior cruciate ligament reconstruction. However, these methods describe the global shape of these bones and do not focus on recognizing landmarks that are clinically valuable, such as the TT. Other studies have shown the superiority of measuring anatomic metrics on 3D models over 2D imaging.[8,9] Sieberer et al.[10] showed that a 3D method of measuring TT-TG using semiautomatic landmark placement could be used to correct scanner-leg alignment that caused errors when measuring in 2D. The purpose of this study was to assess the inter- and intrarater reliability of 21 anatomical landmarks initially placed with an AI algorithm and then manually verified with human input. We hypothesized that the integration of AI-generated landmarks with manual validation would generate a landmark dataset used in calculating anatomic metrics with high inter-rater and intrarater reliability.

Methods

Patient Selection

CT images in the form of Digital Imaging and Communication in Medicine (DICOM) files for 247 patients ages 45 to 55 years at the 144-month visit were initially selected. Approximately one half of these participants experienced progression of patellofemoral osteoarthritis, defined as an increased cartilage score in the patellofemoral compartment on MRI over 2 years. Members of the team who were segmenting 3D models and placing landmarks were blinded to the clinical history and outcome of all patients. Of the initial 247 patients, 30 patients were randomly selected for this study.

Imaging Protocol

The Multicenter Osteoarthritis Study (MOST) is a cohort study funded by the National Institutes of Health of on persons ages 45 years and older with or at high risk of knee osteoarthritis.[11] Participants were imaged at 2 different sites using dual-energy CT. The University of Iowa used a Siemens SOMATOM Force scanner (80/150 kVp, 250 mAs, 0.8-mm pitch, tin filtration at 150 kVp, rotation speed 15 milliseconds) and the University of Alabama at Birmingham used a GE Discovery CT750HD scanner (80/140 kVp, 260 mAs, 0.9 mm pitch, 0.8 s exposure, rotation speed 50 milliseconds). The raw projection data underwent reconstruction under the parameters described by Jarraya et al.[12]

Autosegmentation

All CT scans of knees of participants from MOST were segmented in Simpleware ScanIP using the CT scans of the knee AI algorithm. This commercially available machine-learning algorithm was already available under the Simpleware AS Ortho/CMF module and was not trained by the authors. The algorithm automatically placed 19 predetermined anatomic landmarks on the femur, tibia, and patella (Fig 1, Table 1). We also added 2 landmark markers for the anterior edge of the tibial plateau and center of the TG because these were required to calculate anatomic metrics for a total of 21 landmarks (Table 1). These landmarks were currently not available under the default package and therefore had to be manually placed. For each knee, the AI-placed landmark coordinates were exported as a comma separated value (.csv) file.

Manual Landmark Review

The 2 reviewers (R.H. and A.M.) were given written instructions describing where to place each landmark. Then, they were given a 1-hour training session as a group and were shown how to place each landmark. After placing all 21 landmarks on 5 practice knees, they were given feedback on accuracy and shown where the landmarks should have ideally been placed. They separately verified all AI-generated landmarks on the 30 knee models in SimpleWare ScanIP and moved them when necessary. In addition, they manually placed the two landmarks in the center of the TG and the anterior edge of the tibial plateau. Landmark placements for each knee were exported as comma separated values files. After 2 weeks, one of the reviewers (R.H.) repeated the process for the same dataset, creating a total of three datasets of landmarks for all 30 knees.

Statistical Analysis

The 3 created datasets, which included the 2 initial placements, and the repeated placement, were used for further analysis. For each AI-placed dataset, the mean Euclidean distance of manual landmark displacement was calculated. Mean absolute disagreement between and within raters was calculated in proximodistal, mediolateral, and anteroposterior direction using the other landmarks. In addition, root mean squared disagreement and mean of disagreement in Euclidean distance were calculated.

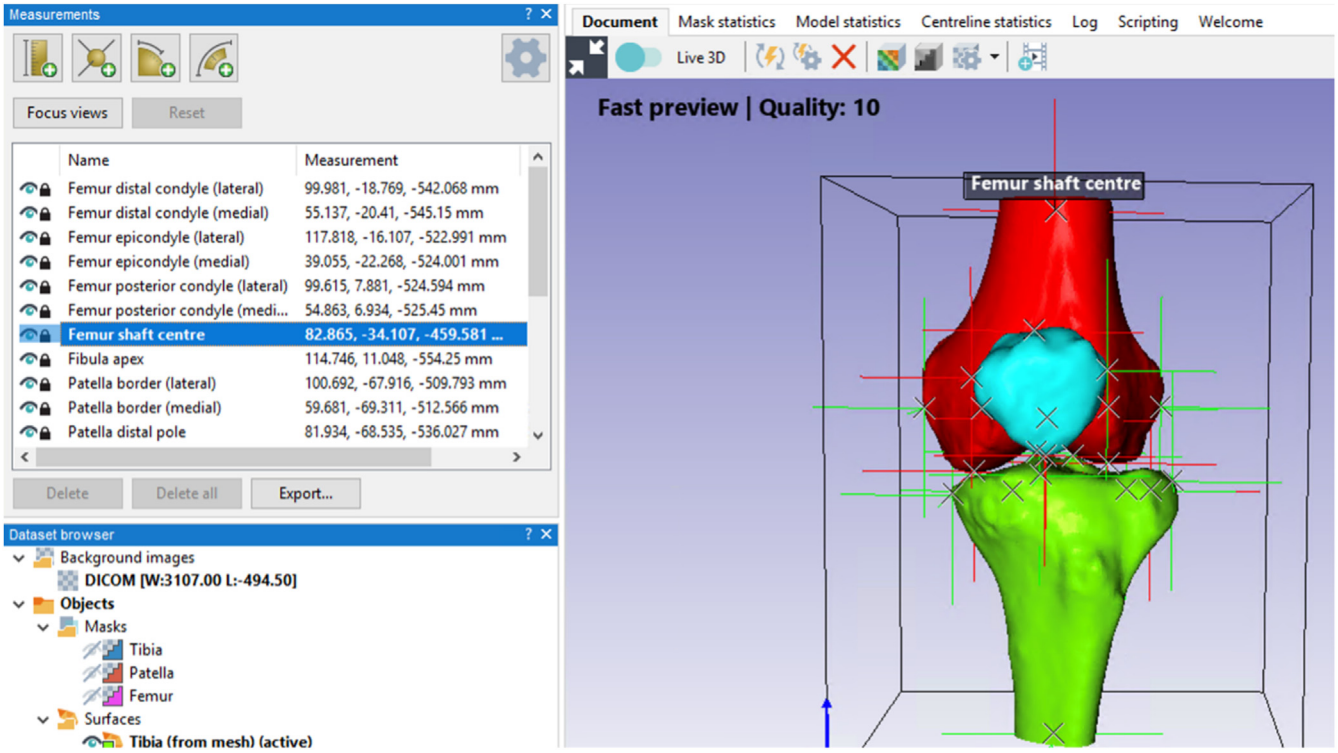

Fig 1. User interface of ScanIP landmark placement. All CT scans of the knee were segmented in Simpleware ScanIP using the CT knee artificial intelligence algorithm. In total, 21 anatomic landmarks were placed on the femur, tibia, and patella. These landmarks were able to be manually dragged around the bone models. (CT, computed tomography.)

Intraclass correlation coefficients (ICCs) were calculated for inter- and intrarater reliability as single measurement, 2-way random and mixed, respectively. Landmark coordinates were translated and referenced to their respective bone centroid to account for different positioning in image space and their respective Euclidian distance were calculated. ICCs and 95% confidence intervals were calculated for these distances. ICCs were evaluated according to Cicchetti et al.[13] (1994) with <0.40 regarded as poor, 0.40 to <0.60 as fair, 0.60 to <0.75 as good, and ≥ 0.75 as excellent.

Results

Of the 19 semiautomated landmarks placed, all had excellent inter-rater reliability (Table 2). The tibial and femur shaft centers had an ICC of 1, indicating no difference in position. Fifteen had an ICC between 0.90 and 0.99, and the tibial tuberosity had an ICC of 0.87. The 2 manually placed landmarks, the tibial plateau and TG, had excellent ICC scores of 0.97 and 0.96, respectively. Intrarater reliability score was 1 for 16 of the 19 semiautomated landmarks and between 0.90 and 0.99 for the remaining three semiautomated landmarks. The manual tibial plateau and TG landmarks had excellent intrarater reliabilities of 0.91 and 0.96, respectively.

The landmarks with the lowest inter-rater disagreement for Euclidean distance were the femoral and tibial shaft centers at 0 mm, whereas the greatest was the lateral femoral epicondyle at 6.70 $\pm$ 4.60 mm. In terms of intrarater disagreement of Euclidean distance, the posterior femoral condyles, femoral and tibial shaft centers, patella borders, distal patella pole, tibia condyles, tibia intercondylar tubercles, and medial posterior femoral condyle all had disagreements of 0 mm. The greatest intrarater disagreement was found in the tibial plateau at 5.14 $\pm$ 7.00 mm. All interrater and intra-rater disagreements can be found in Table 3.

Discussion

All 21 landmarks studied had excellent inter- and intrarater reliability. Inter-rater reliability ranged from 1 (femur and tibial shaft centers) to 0.87 (tibial tuberosity). Intrarater reliability ranged from 1 (16 landmarks) to 0.91 (tibial plateau). In this study of 30 3D knee models and 21 anatomic landmarks, we established a reliable semiautomated method for generating landmarks with a mixture of human and AI input. This study provides a reliable methodology for measuring metrics in 3 dimensions.

The inter-rater was generally lower than intrarater reliability, indicating that there were some discrepancies between how raters interpreted the landmark

Table 1. Landmark Descriptions, Intraclass Correlation, and Error

Landmark	Description	Semiautomated
Distal femoral condyle (M)	Most distal point of medial femoral condyle	Y
Distal femoral condyle (L)	Most distal point of lateral femoral condyle	Y
Femoral epicondyle (M)	Most prominent protrusion on medial distal femur	Y
Femoral epicondyle (L)	Most prominent protrusion on lateral distal femur	Y
Posterior femoral condyle (M)	Most posterior point of medial femoral condyles	Y
Posterior femoral condyle (L)	Most posterior point of lateral femoral condyles	Y
Femoral shaft center	Midpoint of a circle fitted around the posterior femoral shaft at its proximal end	Y
Patellar border (M)	Most medial point of patella	Y
Patellar border (L)	Most lateral point of patella	Y
Patellar pole (P)	Most proximal point of patella	Y
Patellar pole (D)	Most distal point of patella	Y
Tibial condyle (M)	Most medial point of tibia condyle	Y
Tibial condyle (L)	Most lateral point of tibia condyle	Y
Tibial intercondylar tubercle (M)	Most prominent point of medial intercondylar tubercle	Y
Tibial intercondylar tubercle (L)	Most prominent point of lateral intercondylar tubercle	Y
Posterior tibial condyle (M)	Most posterior point of medial tibial condyle	Y
Posterior tibial condyle (L)	Most posterior point of lateral tibial condyle	Y
Tibial shaft center	Midpoint of a circle fitted around the posterior tibial shaft at its distal end	Y
Tibial tuberosity	Center of patellar tendon attachment	Y
Trochlear groove	Deepest point of the trochlear groove	N
Tibial plateau	Anterior-most point of the tibial plateau	N

NOTE. The algorithm automatically placed 19 predetermined anatomic landmarks on the femur, tibia, and patella. The anterior edge of the tibial plateau and center of the trochlear groove were manually added, for a total of 21 landmarks studied. ICC and RMS are rounded to the nearest 2 decimal points.

D, distal; ICC, intraclass correlation; L, lateral; M, medial; N, no; P, proximal; RMS, root mean squared; Y, yes.

definition. Even though the interrater reliability was excellent, anyone implementing a similar manual or semiautomatic procedure needs to be aware that their definition of landmarks might differ from ours. For example, 2 people placing a landmark on the TG may place theirs slightly superior or inferior to each other's. With the advent of a completely automated workflow, this becomes less of an issue. Furthermore, a completely automated pipeline for metrics would solve the current issue of different interpretations of how to

Table 2. Inter- and Intrarater Reliability Shown as ICCs

Landmark	Inter-rater reliability	Intrarater reliability
Distal femoral condyle (M)	0.96 (0.92-0.98)	1.00 (1.00-1.00)
Distal femoral condyle (L)	0.95 (0.91-0.98)	1.00 (1.00-1.00)
Femoral epicondyle (M)	0.98 (0.97-0.99)	1.00 (1.00-1.00)
Femoral epicondyle (L)	0.96 (0.93-0.98)	1.00 (0.99-1.00)
Posterior femoral condyle (M)	0.96 (0.92-0.98)	1
Posterior femoral condyle (L)	0.95 (0.91-0.97)	1
Femoral shaft center	1	1
Patellar border (M)	0.97 (0.95-0.98)	1
Patellar border (L)	0.98 (0.97-0.99)	1
Patellar pole (P)	0.98 (0.96-0.99)	0.99 (0.99-1.00)
Patellar pole (D)	0.99 (0.98-0.99)	1
Tibial condyle (M)	0.99 (0.98-0.99)	1
Tibial condyle (L)	0.99 (0.98-0.99)	1
Tibial intercondylar tubercle (M)	0.99 (0.98-0.99)	1
Tibial intercondylar tubercle (L)	0.99 (0.98-0.99)	1
Posterior tibial condyle (M)	0.94 (0.88-0.97)	1
Posterior tibial condyle (L)	0.99 (0.98-0.99)	0.99 (0.97-0.99)
Tibial shaft center	1	1
Tibial plateau	0.97 (0.94-0.98)	0.91 (0.82-0.96)
Tibial tuberosity	0.87 (0.75-0.93)	0.93 (0.87-0.97)
Trochlear groove	0.96 (0.91-0.98)	0.96 (0.92-0.98)

NOTE. ICCs were calculated for inter-rater and intrarater reliability as single measurement, 2-way random and mixed, respectively. ICC and RMS are rounded to the nearest 2 decimal points.

D, distal; ICC, intraclass correlation; L, lateral; M, medial; P, proximal; RMS, root mean squared.

Table 3. Inter-rater (IRR) and Intrarater (IAR) Disagreement

Landmark	IRR ML/mm	IRR AP/mm	IRR IS/mm	IRR Euclidean/mm	IAR ML/mm	IAR AP/mm	IAR IS/mm	IAR Euclidean/mm
Distal femoral condyle (M)	1.01 ± 1.31	1.54 ± 2.11	0.17 ± 0.26	2.00 ± 2.37	0.10 ± 0.56	0.25 ± 1.35	0.03 ± 0.17	0.56 ± 0.27
Distal femoral condyle (L)	1.11 ± 1.25	2.06 ± 2.82	0.30 ± 0.60	2.70 ± 2.86	0.08 ± 0.42	0.40 ± 2.16	0.09 ± 0.51	0.42 ± 0.41
Femoral epicondyle (M)	0.38 ± 0.31	1.38 ± 1.00	1.84 ± 1.74	2.67 ± 1.55	0.03 ± 0.15	0.08 ± 0.35	0.42 ± 1.67	0.15 ± 0.43
Femoral epicondyle (L)	0.6 ± 0.75	2.94 ± 3.26	5.49 ± 40	6.70 ± 4.60	0.12 ±0.34	0.78 ± 2.04	0.46 ± 1.60	0.34 ± 0.95
Posterior femoral condyle (M)	1.56 ± 1.41	0.18 ± 0.21	0.98 ± 1.4	2.05 ± 1.79	0	0	0	0
Posterior femoral condyle (L)	1.18 ± 1.35	0.14 ± 0.23	0.56 ± 0.99	1.48 ± 1.54	0	0	0	0
Femoral shaft center	0	0	0	0	0	0	0	0
Patellar border (M)	0.19 ± 0.28	0.53 ± 0.73	0.86 ± 1.38	1.15 ± 1.5	0	0	0	0
Patellar border (L)	0.24 ± 0.31	0.93 ± 1.34	1.14 ± 1.45	1.63 ± 1.88	0	0	0	0
Patellar pole (P)	0.81 ± 1.21	0.33 ± 0.53	0.18 ± 0.45	0.95 ± 1.36	0.12 ± 0.58	0.05 ± 0.22	0.06 ± 0.27	0.58 ± 0.15
Patellar pole (D)	0.68 ± 1.15	0.32 ± 0.59	0.07 ± 0.14	0.78 ± 1.29	0	0	0	0
Tibial condyle (M)	0.27 ± 0.42	1.23 ± 1.80	0.71 ± 0.89	1.60 ± 1.94	0	0	0	0
Tibial condyle (L)	0.21 ± 0.35	1.58 ± 2.01	0.43 ± 0.74	1.76 ± 2.08	0	0	0	0
Tibial intercondylar tubercle (M)	0.99 ± 0.93	0.55 ± 0.41	0.26 ± 0.25	1.30 ± 0.87	0	0	0	0
Tibial intercondylar tubercle (L)	0.90 ± 0.69	0.64 ± 0.59	0.21 ± 0.17	1.24 ± 0.76	0	0	0	0
Posterior tibial condyle (M)	1.65 ± 1.53	0.31 ± 0.34	1.31 ± 1.25	2.31 ± 1.79	0	0	0	0
Posterior tibial condyle (L)	1.02 ± 1.32	0.43 ± 0.70	0.39 ± 0.58	1.24 ± 1.55	0.10 ± 0.39	0.08 ± 0.30	0.24 ± 0.98	0.39 ± 0.28
Tibial shaft center	0	0	0	0	0	0	0	0
Tibial plateau	2.92 ± 2.39	1.29 ± 1.03	2.21 ± 1.49	4.37 ± 2.21	6.25 ± 5.14	1.14 ± 1.14	2.06 ± 1.85	5.14 ± 7.00
Tibial tuberosity	1.07 ± 1.18	1 ± 0.96	1.24 ± 1.62	2.27 ± 1.85	1.14 ± 1.02	0.87 ± 0.61	1.49 ± 1.28	1.02 ± 2.38
Trochlear groove	0.57 ± 0.36	1.67 ± 1.23	1.43 ± 1.13	2.40 ± 1.52	0.79 ± 0.69	1.61 ± 1.10	1.58 ± 1.30	0.69 ± 2.59

NOTE. Mean Euclidean distance of manual landmark displacement was calculated. Mean absolute disagreement between and within raters was calculated in proximodistal, mediolateral, and anteroposterior direction using the other landmarks. In addition, RMS disagreement and mean of disagreement in Euclidean distance were calculated.

D, distal; ICC, intraclass correlation; L, lateral; M, medial; P, proximal; RMS, root mean squared.

measure existing 2D metrics, enabling consistent industry-wide thresholds. Until then, the reliability of the methods outlined in this study are only as good as the training that each landmark reviewer receives before placing landmarks.

There has been a recent sudden increase of interest in AI's capabilities across numerous medical fields, and orthopaedics is no exception.[14] AI-based segmentation tools are designed to minimize time manually segmenting scans, thereby decreasing procedural costs and enhancing efficiency. The resulting 3D models have far-reaching implications, from helping produce personalized implants in arthroplasty, to optimizing femoroacetabular configuration to reduce impingement during hip arthroscopy, to visualizing frequent fracture patterns in orthopedic trauma.[15-17] Our results show that combining AI-generated landmarks with human input offers a promising avenue to enable comprehensive metric calculations. In our group, we have a dedicated research team of medical and graduate students, as well as a fully in-house engineering and 3D printing services program within our orthopaedics department. For practical use, it is important to consider that at this time, most surgeons do not have a dedicated research team who can export patient DICOM images to segmentation software, run the AI algorithm to create a 3D model, and adjust landmarks as needed. However, with the growing utility of 3D printing, one can envision that many centers will see the advantage of hiring engineers who can streamline this process. In femoroacetabular impingement, some hip-preservation surgeons have started to collaborate with device companies to perform 3D analysis of the hip, such as in the HipMap FAI analysis (Stryker).[17,18] Nerys-Figueroa et al.[19] have shown that 2D radiographs underestimate lateral center-edge angle measurements compared with the HipMap's 3D CT calculations. Similarly, we anticipate that advancements in 3D analysis of the knee can become an integral component of a surgeon's toolkit.

When describing knee pathology, traditional 2D measurements face inherent vulnerabilities as the result of scanner alignment axis and slice selection. Anatomic metrics in the knee can face distortions on the basis of degree of leg abduction in the scanner and can be different when measured on MRI compared with CT scans because of relative varus positioning in MRI.[3,4,20] Accurate assessment of anatomical metrics is fundamental when counseling patients and identifying a surgical plan. Measurement on 3D models can bypass the quandary of measuring the distance between 2 landmarks that do not line up in the axial plane. For example, authors have found that measuring TT-TG on 3D models has a greater inter-rater agreement compared with measurements done on conventional 2D slices.[8,9] Sieberer et al.[10] used seven 3D knee landmarks described in this article to correct alignment errors in TT-TG distance. Measuring TT-TG in 3D can help better delineate which patients truly have a lateralized tibial tubercle and may benefit the most from a tibial tubercle osteotomy. The senior author (J.P.F.) already routinely only uses 3D TT-TG in his practice, along with 3D visualization of trochlear dysplasia.[21-23] However, this requires further study to understand if this difference is seen in surgical practice.

The problematic nature of 2D imaging has also been identified beyond the patellar instability literature. Posterior tibial slope (PTS), which has an important role in total knee arthroplasty, high tibial osteotomy, and anterior cruciate ligament reconstruction, is routinely measured on lateral radiographs of the lower limb.[24] However, measuring the PTS at different diaphyseal axes with varying lengths below the tibial plateau has been found to lead to different results, with shorter radiographs yielding an overestimation of the PTS.[24] This effect also leads to lower PTS measurements on MRI, in combination with the effect that malpositioning during imaging has on PTS.[25] Lateral radiographs are vulnerable to PTS errors of up to 14 degrees as the result of tibial rotation, whereas CT scans yielded errors of less than 3°.[26] Bixby et al.[27] found that 10° of leg abduction or adduction led to a decrease or increase, respectively, of 3 degrees of PTS. In contrast to measuring anatomic metrics in 2D, 3D models offer a promising avenue to mitigate these errors, as they are resistant to malpositioning. A better understanding of which patients truly have a greater PTS could pinpoint who may be at a greater risk of ACL reconstruction failure without either an anterior closing-wedge or posterior opening-wedge osteotomy.

Limitations

There are several limitations to consider in our study. We did not directly compare the intraclass correlation between our 3D landmarks and 2D landmarks. Furthermore, 2 of our landmarks were generated manually, as the segmentation algorithm did not automatically identify them. In addition, our methods relied on a single segmentation algorithm from a 3D image segmentation software, which is commercially available but may not be available for many surgeons. Moreover, this method was tested on 30 knees imaged from participants in MOST, a study of middle-aged and older persons with or at risk of knee osteoarthritis. We studied knees without severe osteoarthritis at the time of CT scan, but were blinded to the clinical outcomes of the participants and could not correlate landmark reliability with pathology. We are currently conducting further research to correlate metrics generated by landmarks with their clinical outcomes. We believe that our results can be generalized to other populations of knees, but more studies should be conducted to better

understand its reliability in dysplastic or diseased knees. Of note, Sieberer et al.[10] used this 3D landmark method to calculate TT-TG in a patellofemoral instability population. Finally, we are unaware how the technical parameters for the imaging used in this study could affect the reliability of our results.

Conclusions

There was excellent agreement on the locations of all 21 landmarks evaluated in this study.

Disclosures

The authors declare the following financial interests/personal relationships which may be considered as potential competing interests: J.P.F. reports a relationship with Linvatec Corporation that includes consulting or advisory. N.A.S. reports a relationship with Pacira Biosciences, Trice Medical, and Professional Medical Consulting that includes consulting or advisory. All other authors (N.P., J.Si., A,M., R-M.H., S.D., R.G., J.L., J.St.) declare that they have no known competing financial interests or personal relationships that could have appeared to influence the work reported in this paper.

Funding

MOST was funded by the National Institutes of Health grants to the University of Iowa (U01AG18832 to J. Torner/N.A.S.), University of California-San Francisco (U01AG19069 to M. Nevitt), University of Alabama at Birmingham (U01AG18947 to C. Lewis), and Boston University (U01AG18820 to D.F.).

References

1. Vairo GL, Moya-Angeler J, Siorta MA, Anderson AH, Sherbondy PS. Tibial tubercle-trochlear groove distance is a reliable and accurate indicator of patellofemoral instability. *Clin Orthop Relat Res* 2019;477:1450-1458.
2. Camp CL, Stuart MJ, Krych AJ, et al. CT and MRI measurements of tibial tubercle–trochlear groove distances are not equivalent in patients with patellar instability. *Am J Sports Med* 2013;41:1835-1840.
3. Hinckel BB, Gobbi RG, Filho EN, et al. Are the osseous and tendinous-cartilaginous tibial tuberosity-trochlear groove distances the same on CT and MRI? *Skelet Radiol* 2015;44:1085-1093.
4. Yao L, Gai N, Boutin RD. Axial scan orientation and the tibial tubercle-trochlear groove distance: Error analysis and correction. *AJR Am J Roentgenol* 2014;202:1291-1296.
5. Liao TC, Jergas H, Tibrewala R, et al. Longitudinal analysis of the contribution of 3D patella and trochlear bone shape on patellofemoral joint osteoarthritic features. *J Orthop Res* 2021;39:506-515.
6. Eijkenboom JFA, Tümer N, Schiphof D, et al. 3D patellar shape is associated with radiological and clinical signs of patellofemoral osteoarthritis. *Osteoarthritis Cartilage* 2023;31:534-542.
7. Williams AA, Koltsov JCB, Brett A, He J, Chu CR. Using 3D MRI bone shape to predict pre-osteoarthritis of the knee 2 years after anterior cruciate ligament reconstruction. *Am J Sports Med* 2023;51:3677-3686.
8. Nha K, Nam YJ, Shin MJ, et al. Referencing the trochlear groove based on three-dimensional computed tomography imaging improves the reliability of the measurement of the tibial tuberosity-trochlear groove distance in patients with higher grades of trochlea dysplasia. *Knee* 2019;26:1429-1436.
9. Shu L, Ni Q, Yang X, Chen B, Wang H, Chen L. Comparative study of the tibial tubercle-trochlear groove distance measured in two ways and tibial tubercle-posterior cruciate ligament distance in patients with patellofemoral instability. *J Orthop Surg Res* 2020;15:209.
10. Sieberer JM, Park N, Rancu AL, et al. Analyzing alignment error in tibial tuberosity—trochlear groove distance in clinical scans using 2D and 3D methods. *Am J Sports Med* 2024;52:2996-3003.
11. Segal NA, Nevitt MC, Gross KD, et al. The Multicenter Osteoarthritis Study: Opportunities for rehabilitation research. *PM R* 2013;5:647-654.
12. Jarraya M, Guermazi A, Liew JW, et al. Prevalence of intra-articular mineralization on knee computed tomography: The Multicenter Osteoarthritis Study. *Osteoarthritis Cartilage* 2023;31:1111-1120.
13. Cicchetti DV, Guidelines. criteria, and rules of thumb for evaluating normed and standardized assessment instruments in psychology. *Psychol Assess* 1994;6:284-290.
14. Batailler C, Shatrov J, Sappey-Marinier E, Servien E, Parratte S, Lustig S. Artificial intelligence in knee arthroplasty: Current concept of the available clinical applications. *Arthroplasty* 2022;4:17.
15. Kahmann SL, Rausch V, Plümer J, Müller LP, Pieper M, Wegmann K. The automized fracture edge detection and generation of three-dimensional fracture probability heat maps. *Med Eng Phys* 2022;110:103913.
16. Batailler C, Fernandez A, Swan J, et al. MAKO CT-based robotic arm-assisted system is a reliable procedure for total knee arthroplasty: A systematic review. *Knee Surg Sports Traumatol Arthrosc* 2021;29:3585-3598.
17. Ratner D, Kolaczko JG, Jeffers K, et al. Three-dimensional analysis versus two-dimensional slice-based analysis of CT for measuring femoral torsion and its correlation to passive hip range of motion. *Cureus* 2022;14:e29554.
18. Moran J, Jimenez AE. Editorial Commentary: Magnetic resonance imaging may underestimate hip femoral version versus computed tomography scan: both may be optimized using 3-dimensional imaging. *Arthroscopy* 2024;40:2411-2412.
19. Nerys-Figueroa J, Maldonado D, Parsa A, Quesada-Jimenez R, Kahana-Rojkind AH, Domb BG. The measurement of the lateral center-edge angle is underestimated on radiographs compared with three-dimensional computed tomography. *Arthrosc Sports Med Rehabil* 2024;7:101005.
20. Ho CP, James EW, Surowiec RK, et al. Systematic technique-dependent differences in CT versus MRI measurement of the tibial tubercle-trochlear groove distance. *Am J Sports Med* 2015;43:675-682.

21. Sieberer JM, Park N, Manafzadeh AR, et al. Visualization of trochlear dysplasia using three-dimensional curvature analysis in patients with patellar instability facilitates understanding and improves the reliability of the entry-point to trochlea groove angle. *Arthrosc Sports Med Rehabil.* 2024;7:101010.
22. Schneble CA, Yu K, Venkadesan M, et al. Three-dimensional imaging of the patellofemoral joint improves understanding of trochlear anatomy and pathology and planning of realignment. *Arthroscopy* 2025;41:130-140.
23. Beitler BG, Sieberer J, Islam W, et al. The morphologic patella entry point into the proximal trochlea is more lateral in recurrent dislocators than controls as measured by entry point-trochlear groove angle. *Arthroscopy* 2025;41:703-712.
24. Faschingbauer M, Sgroi M, Juchems M, Reichel H, Kappe T. Can the tibial slope be measured on lateral knee radiographs? *Knee Surg Sports Traumatol Arthrosc* 2014;22:3163-3167.
25. Gwinner C, Fuchs M, Sentuerk U, et al. Assessment of the tibial slope is highly dependent on the type and accuracy of the preceding acquisition. *Arch Orthop Trauma Surg* 2019;139:1691-1697.
26. Kessler MA, Burkart A, Martinek V, Beer A, Imhoff AB. Development of a 3-dimensional method to determine the tibial slope with multislice-CT. *Z Orthop Ihre Grenzgeb* 2003;141:143-147 [in German].
27. Bixby EC, Tedesco LJ, Confino JE, Mueller JD, Redler LH. Effects of malpositioning of the knee on radiographic measurements: The influence of adduction, abduction, and malrotation on measured tibial slope. *Orthop J Sports Med* 2023;11:23259671231164670.